Featured Article

Vibrio cholerae YaeO is a Structural Homologue of RNA Chaperone Hfq that Inhibits Rho-dependent Transcription Termination by Dissociating its Hexameric State

Kamalendu Pal [1], Malti Yadav [1], Sriyans Jain [2], Biplab Ghosh [3], Ranjan Sen [2] and Udayaditya Sen [1]

*1 - **Crystallography and Molecular Biology Division,** Saha Institute of Nuclear Physics, HBNI, 1/AF Bidhan Nagar, Kolkata 700064, India*
*2 - **Laboratory of Transcription,** Center for DNA Fingerprinting and Diagnostics, Tuljaguda Complex, 4-1-714 Mouzamjahi Road, Nampally, Hyderabad 500 001, India*
*3 - **High Pressure & Synchrotron Radiation Physics Division,** Bhabha Atomic Research Centre, Trombay, Mumbai 400085, India*

Correspondence to Udayaditya Sen: *Crystallography and Molecular Biology Division, Saha Institute of Nuclear Physics, 1/AF Bidhan Nagar, Kolkata 700 064, India.* udayaditya.sen@saha.ac.in
https://doi.org/10.1016/j.jmb.2019.09.019
Edited by M. Gottesman

Abstract

Rho-dependent transcription termination is a well-conserved process in bacteria. The Psu and YaeO proteins are the two established inhibitors of the ATP-dependent RNA helicase Rho protein of *Escherichia coli*. Here, we show a detailed sequence and phylogenetic analysis demonstrating that *Vibrio cholerae* YaeO (*Vc*YaeO) is significantly distinct from its *E. coli* counterpart. *Vc*YaeO induces significant growth defect on *in vivo* expression and inhibits *in vitro* functions of the *V. cholerae* Rho on directly binding to the latter. Through various biophysical techniques, we showed that interaction of *Vc*YaeO disrupts the oligomeric state of the *Vc*Rho. Structure of *Vc*YaeO solved at 1.75 Å resolution, the first crystal structure of a YaeO protein, demonstrates a beta-sandwich fold distinct from the NMR structure of the *Ec*YaeO. Interestingly, *Vc*YaeO structurally resembles the Hfq protein, and like the latter, it exhibits ssDNA/RNA-binding properties. Docking studies demonstrate probable interactions of *Vc*YaeO with *Vc*Rho and mode of inhibition of RNA binding to Rho. We propose that *Vc*YaeO inhibits the function of the Rho protein via disruption of the latter's hexameric assembly and also likely by sequestering the RNA from the Rho primarybinding sites.

Introduction

A successful and precise transcription termination is required for regulation of bacterial gene expression. The transcription termination in bacteria is primarily of two types: factor-independent and factor-dependent [1]. A stem-loop structure with GC-rich self-complementary region followed by U-rich track causes dissociation of the elongation complex (EC) in the factor-independent termination [2]. Conversely, the factor-dependent termination requires the action of a hexameric helicase Rho [3]. The Rho protein is a conserved hexameric RNA-dependent helicase that binds to the rho utilizing sites (*rut*) on the nascent RNA and translocates in the 5′ to 3′ direction along the RNA using the energy from ATP hydrolysis until it reaches the transcription EC [4,5].

Until now, two inhibitors of Rho-dependent transcription termination have been identified. The *psu* of the satellite bacteriophage P4 encodes a dimeric 21.3 kDa protein that inhibits Rho through direct binding [6]. Psu efficiently inhibits Rho-dependent terminations by exerting a mechanical impediment to the latter's translocase activity [7]. We have previously reported the crystal structure of Psu that exhibits a novel fold and unique “V”-shaped knotted structure [8]. The other inhibitor, YaeO, is a 9 kDa acidic protein that was first identified from *Escherichia coli* (*Ec*YaeO). YaeO has no obvious sequence similarities with any other protein. *In vivo, Ec*YaeO reduces the efficiency of the Rho-dependent termination at the t_{L1} terminator [9]. *Ec*YaeO binds tightly to *E. coli* Rho (*Ec*Rho), but the exact nature of this interaction is unknown. NMR structure indicated that

*Ec*YaeO is composed of an N-terminal helix followed by a seven-stranded β-sandwich [10]. *Ec*YaeO exhibits structural similarity with Hfq (host factor gene for bacteriophage Q beta) protein [10], which is an RNA chaperone that binds small regulatory RNA and mRNAs [11,12].

Vibrio cholerae is the causative organism of severe diarrheal disease cholera in the developing countries affecting millions of people [13]. YaeO of *V. cholerae* (*Vc*YaeO), encoded by the *yaeO* gene, is a member of a family of Rho-dependent transcription termination inhibitors. Detailed sequence and phylogenetic analysis indicate that *Vc*YaeO is distinctly different from its *E. coli* counterpart (Fig. 1a). They belong to different branches of the phylogenetic tree, and their sequence identity is also quite low (24%). Here, we have demonstrated direct binding of *Vc*YaeO with *Vc*Rho using various biochemical and biophysical tools. Size exclusion chromatography (SEC) and dynamic light scattering (DLS) techniques convincingly indicated that *Vc*YaeO induces dissociation of the hexameric state of the *Vc*Rho. We have determined the crystal structure of *Vc*YaeO at 1.75 Å, which exhibited a beta-sandwich fold. Inner layer of the beta-sandwich was observed to be packed by hydrophobic residues. DALI search indicated a close structural homology of *Vc*YaeO with Hfq proteins rather than *Ec*YaeO. Consistent with this prediction, we demonstrated that like Hfq, *Vc*YaeO interacts with RNA and ssDNA having G- and C-rich sequences. Based on the biochemical properties of *Vc*YaeO and the structural model of *Vc*YaeO:*Vc*Rho complex, we propose that *Vc*YaeO inhibits the function of Rho by dissociating latter's hexameric state likely via sequestering the RNA from the Rho primarybinding site.

Results

Sequence analysis of *Vc*YaeO

*Vc*YaeO codes for a 9.3 kDa protein, and its primary sequence has no apparent resemblance with other proteins. YaeO appears to be a member of a family of inhibitors of Rho-dependent transcription termination. YaeO-related proteins are present in several species of Gram-negative and Gram-positive bacteria. Phylogenetic analyses with more than hundred nonredundant (NR) sequences of YaeO, identified through BLAST search, revealed that *Ec*YaeO- and *Vc*YaeO-type proteins fall in separate clusters (Supplementary Fig. S1 and Fig. 1a). Multiple sequence alignment of YaeO sequences (Fig. 1a) showed that only four acidic residues and two cysteine residues are conserved (Fig. 1a and b) among YaeOs of different species. Furthermore, a number of regions (underlined in blue in Fig. 1a) are widely different between *Vc*YaeO- and *Ec*YaeO-type proteins pointing toward their distinct nature.

*Vc*YaeO remains as dimer in solution

Although *V. cholerae* is a Gram-negative bacteria, *Vc*YaeO is quite different from its *E. coli* counterpart.

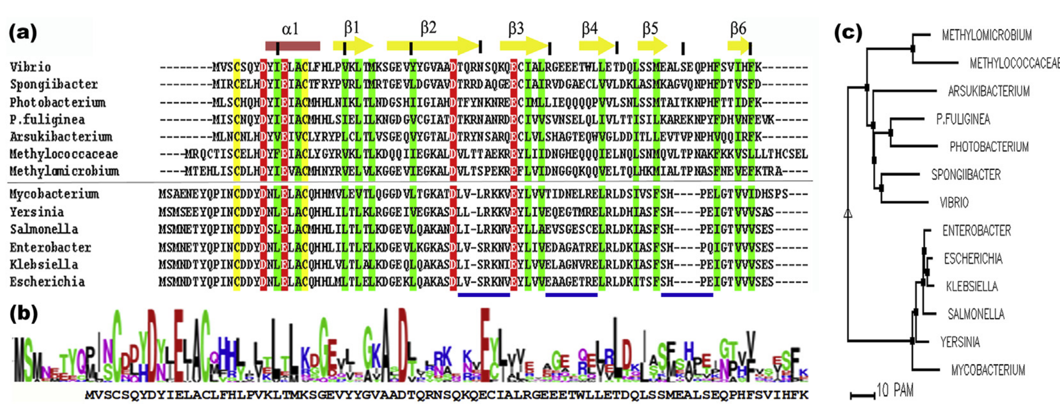

Fig. 1. Sequence alignment and phylogenetic analysis of YaeO. (a) Sequence alignment of *Vibrio cholerae* YaeO with twelve homologous proteins (having less than 60% sequence identity) indicating two distinct groups (separated by thin gray line). Blue underlined regions differ significantly between the two groups. Only four acidic residues (highlighted in red) and two cysteines (yellow) are conserved throughout the species. Similar hydrophobic residues are highlighted in green. Protein sequences used to generate the alignment and their UniProt accession codes are *V. cholerae*: A0A0H3ADN9; *Spongiibacter* sp: A0A2D7WHH1; *Photobacterium phosphoreum*: A0A0B7JK74; *Pseudoalteromonas fuliginea*: A0A063KWA5; *Arsukibacterium ikkense*: A0A0M2V2K1; *Methylococcaceae bacterium*: A0A257NBF5; *Methylomicrobium album*: H8GH92; *Mycobacterium tuberculosis*: A0A1K3H6J5; *Yersinia pestis*: A0A0E1NSG3; *Salmonella typhimurium*: E8XIQ7; *Enterobacter cloacae*: A0A144RC60; *Klebsiella pneumoniae*: A0A333FHM5; and *Escherichia coli*: P0AFW8. (b) A consensus sequence logo generated based on (a) is depicted. (c) Phylogenetic tree with these sequences depicts that *Vc*YaeO is a distant homolog of *E. coli* YaeO and belongs to a separate branch.

To explore the interactions of *Vc*YaeO with *Vc*Rho, we have cloned *Vc*YaeO into *E. coli* XL1-Blue and overexpressed in BL21 (DE3) strain. *Vc*YaeO was purified to homogeneity though Ni-NTA affinity chromatography followed by SEC (Supplementary Fig. S2). *Vc*YaeO has been observed to be highly precipitation prone on storage. Fresh preparation of *Vc*YaeO shows a single band, both in reducing and nonreducing SDS-PAGE, and elutes as a dimer in SEC (Supplementary Fig. S3a). However, on storage at 4 °C, the protein tends to precipitate. SEC of this sample clearly shows two dominant peaks. One peak is close to the peak of blue dextran indicating formation of a high molecular weight species, and the location and shape of the other peak indicate a mixture of dimer and higher oligomer(s) (Supplementary Fig. S3b). Analysis of this sample by nonreducing SDS-PAGE indicates the formation of higher order oligomers (Supplementary Fig. S3c). Interestingly, incubation of freshly prepared *Vc*YaeO with iodoacetamide/TCEP prevents the formation of high-order oligomer, thus retaining the dimeric state (Supplementary Figs. S3b and S3c). Hence, this iodoacetamide/TCEP-treated sample was used for crystallization and other studies.

The crystal structure of *Vc*YaeO and comparative analysis

Because the sequence of *Vc*YaeO is significantly different from that of *Ec*YaeO, we proceeded to solve the structure of *Vc*YaeO to understand whether it inhibits the Rho function via a distinct mechanism. Initial crystallization trials of *Vc*YaeO yielded small sea urchin−like crystals that were difficult to grow larger. *Vc*YaeO is precipitation prone, and a nondenaturing SDS-PAGE showed the presence of dimer and higher order oligomers (Supplementary Fig. S3c). *Vc*YaeO contains three cysteine residues, and their location in homologous structure rules out the formation of disulfide bond between any two pairs. Unpaired free cysteine(s) are, therefore, the most probable candidate(s) for oligomerization, rendering the protein precipitation prone. We solved this problem by treating the protein with iodoacetamide (Supplementary Figs. S3b and S3c). Subsequent crystallization trials with iodoacetamide and 10% ethylene glycol as additive produced rod-shaped crystals.

The *Vc*YaeO protein structure could not be solved using the published NMR models of *Ec*YaeO (PDB code: 1SG5). This indicates that *Vc*YaeO probably has distinct structural features. The structure of *Vc*YaeO was solved using the coordinates of Hfq protein (PDB code: 4PNO) with two molecules in the asymmetric unit. The structure was refined well with excellent stereochemical parameters that were consistent with the quality of the diffraction data (Table 1). Both the *Vc*YaeO molecules of the asymmetric unit have well-defined electron density except for the four N-terminal residues and they superpose well (RMSD value 0.15 Å for 68 matching C_α atoms). Each monomer of *Vc*YaeO exhibited a beta-sandwich−like structure, comprising of the N-terminal solitary alpha helix followed by six antiparallel beta-strands (Fig. 2a). The longest strand β2 contains 14 residues and spans two sides of the β-sandwich (designated as $\beta2^N$ and $\beta2^C$). One face of the sandwich is formed by antiparallel strands $\beta2^N$, β1, β5, and β6, while the other face is formed by $\beta2^C$, β3, and β4, respectively (Fig. 2a). Assignment of the secondary structural elements relative to the primary sequence is shown in Fig. 1a. Sequence identity between *Vc*YaeO and YaeO of different species is significantly low even in the regions with matching secondary structures. However, the residues that pack inner layer of the sandwich are similar in nature and contain mostly small hydrophobic residues (Figs. 1a and 2b).

Once the structure of *Vc*YaeO was solved, we were curious to know why the NMR model of *Ec*YaeO failed to produce any solution in molecular replacement (MR) calculations. A search for structural homologs in the DALI server [14] identified several proteins (Table 2) including the small ribonucleoprotein, Hfq. Interestingly, all of them are RNA/ssDNA and nucleotide-binding proteins exhibiting Z-scores 9.6 to 6.5 and RMS deviations 1.8 to 2.5 Å for matching C_α atoms (Table 2). Table 2 also indicates that structurally *Vc*YaeO is widely different from *Ec*YaeO, which explains why the NMR models of the latter failed to solve the structure. Structural superposition revealed that even though their β-strands roughly match, the connecting loops are dissimilar, specifically β1−β2, β2−β3, β4−β5, and β5−β6 loops showed noticeable deviations (Fig. 2c and d). Although the longer size of the loops connecting β2−β3 and β5−β6 in *Vc*YaeO could be because of the insertion of residues, deviations in other loops are purely because of sequence difference. Moreover, *Ec*YaeO has a longer N-terminal loop, and the orientation of the α-helix following it is drastically different. Variable loop sizes and orientation coupled with sequence differences changes the surface properties of *Vc*YaeO distinctly from *Ec*YaeO, which might influence their molecular recognition properties.

The hallmark of Hfq protein is to form stable hexamer either in RNA bound or unbound form [15,16]. Despite having high structural resemblance with Hfq, *Vc*YaeO showed a dimeric form (Fig. 2e and Supplementary Fig. S3). The most important structural difference observed between *Vc*YaeO and Hfq proteins is the presence of an additional β-strand (β6) in YaeO at the C-terminal (Fig. 2c−d). Moreover, β2 and β3, along with the connecting loop, are also quite different in case of YaeO. Interestingly, both of these regions are involved in hexameric contacts and stability of the Hfq proteins. Therefore,

Table 1. Data collection and refinement statistics of *VcYaeO*.

X-ray source	Beamline PX-BL-21, RRCAT, Indore, India
Wavelength (Å)	0.979470
Resolution (Å)	40.92−1.75 (1.78−1.75)
Space group	P1
Cell dimensions, a, b, c (Å); α, β, γ (°)	28.94, 34.36, 42.37; 90.07, 104.48, 105.49
Unique reflections	14,765
Multiplicity	3.3
R_{merge} (%)	5.6 (29.4)
I/σ(I)	15.7 (4.1)
Completeness (%)	96.4 (80.3)
Refinement	
R_{work}/R_{free} (%)	16.64/20.85
RMSD	
Bond length (Å)	0.015
Bond angles (°)	0.807
Ramachandran statistics (%)	
Favored regions	98.67
Allowed regions	1.33
Outliers	0.00
Number of atoms	
Protein	1246
Heteroatom	4
Water	219
Average B-factor (Å^2)	
Protein (main chain) (A/B)	17.79/17.51
Protein (side chain) (A/B)	24.46/24.71
Protein (A/B)	21.17
Heteroatom (201, 202, 301, 302)	32.7, 43.4, 30.3, 30.8
Water	34.87
PDB code	6JIE

these two structural features hinder the formation of hexamer in case of *Vc*YaeO.

Crystal structure of *Vc*YaeO shows two molecules in the asymmetric unit, and they interact with each other to form a dimer (Fig. 2e) that is in accordance with our solution studies. Dimerization of *Vc*YaeO buries about 10% of the total surface area (~500 Å^2 out of total 5200 Å^2) providing a net free energy of interaction—7 kcal/mol as calculated by *PDBe PISA* web server [17]. *Vc*YaeO dimer is mostly stabilized through hydrophobic interactions involving residues Y7, Y9, L12, L15, F16, H17, and V33 (Fig. 2f). Dimeric form of *Vc*YaeO structure is consistent with that observed in solution (Supplementary Fig. S3a).

*Vc*YaeO directly binds to *Vc*Rho

Pull-down assay indicates that VcYaeO binds to VcRho

Full-length *Vc*Rho (*Vc*Rho$_{FL}$) and its N-terminal domain (residues 1−130; *Vc*Rho$_{130}$) were purified by Ni-NTA affinity chromatography followed by heparin column and SEC (Supplementary Fig. S2). Pull-down assays of *Vc*Rho with *Vc*YaeO were performed on the Ni-NTA matrix. Preincubated mixture of His tagged *Vc*Rho$_{FL}$ and *Vc*YaeO (whose 6 × His tag was removed) was allowed to bind to the resin, and after exhaustive wash with different buffers (RB, WB1, and WB2, see Materials and methods), immobilized *Vc*Rho$_{FL}$ was eluted with the elution buffer (EB). Analysis of proteins eluted by EB in a 15% SDS-PAGE showed coelution of *Vc*YaeO with *Vc*Rho$_{FL}$ indicating a direct *Vc*YaeO:*Vc*Rho interaction (Fig. 3a). Binding of *Vc*YaeO was not observed with the resin alone (data not shown), thus ruling out the possibility of any nonspecific adherence to the resins. It was reported earlier that *Ec*YaeO interacts with the N-terminal part of *Ec*Rho [10]. Therefore, we checked the interaction of *Vc*YaeO with *Vc*Rho$_{130}$. SDS-PAGE showed that *Vc*YaeO coeluted with *Vc*Rho$_{130}$ (Fig. 3b), delineating the interactions of *Vc*YaeO with N-terminal of *Vc*Rho. It is to be noted that in both the pull-down experiments, salt concentration used in the wash buffers (WB1 and WB2) were substantially high. However, at these high salt concentration, the dissociation of the *Vc*YaeO:*Vc*Rho complex or *Vc*YaeO:*Vc*Rho$_{130}$ complex is negligible, indicating these complexes are stable.

Binding analyses using native gel electrophoresis

We have further confirmed the direct binding of *Vc*YaeO with *Vc*Rho$_{130}$ by using native PAGE. *Vc*YaeO and *Vc*Rho$_{130}$ were incubated for 30 min before running the gel electrophoresis. Lanes containing only *Vc*YaeO or *Vc*Rho$_{130}$ showed a single band indicating the homogeneity of the preparations, whereas the lane containing *Vc*YaeO and *Vc*Rho$_{130}$ mixture showed two bands (Fig. 3c). The position of

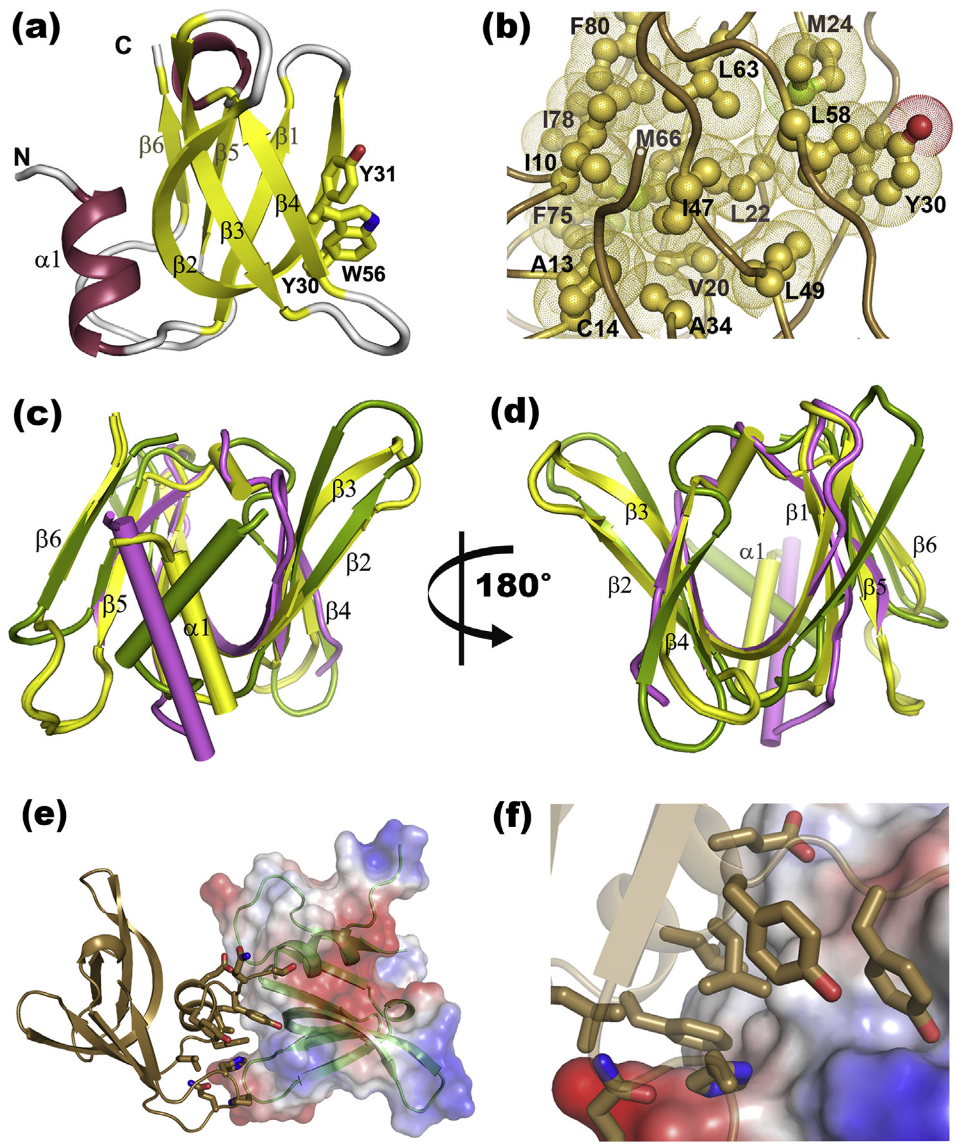

Fig. 2. Structural analysis of *Vc*YaeO. (a) β-sandwich folds of *Vc*YaeO consisting of six antiparallel strands, and N-terminal helix. Aromatic residues, W56, Y30, and Y31 implicated in DNA/RNA binding are shown in sticks. (b) Residues involved in packing of the core of β-sandwich are shown as ball and stick along with their Van der waals surface and labeled. (c) Structural superposition of *Vc*YaeO chain A and B (yellow; RMSD 0.155), *Ec*YaeO (green), and *Escherichia coli* Hfq (magenta); different orientations/size of loops connecting β1–β2, β2–β3, β4–β5, β5–β6, and N-terminal α helix of *Vc*YaeO are evident. (d) 180° rotation of this superposed structure. (e) *Vc*YaeO dimer where one monomer is shown in electrostatic surface. (f) Residues involved in the formation of dimer are represented in sticks and their hydrophobic nature is evident.

one band matches closely with *Vc*Rho_{130}, whereas the position of the other band indicates the formation of a complex between *Vc*YaeO and *Vc*Rho_{130} (Fig. 3c). Because excess of *Vc*Rho_{130} was used, no band for free *Vc*YaeO was observed.

Fluorescence quenching assay and ITC further confirm the binding between VcYaeO and VcRho

The binding affinity of *Vc*YaeO (dimer) with *Vc*Rho_{130} was estimated by monitoring the change in fluorescence of the FITC-labeled *Vc*Rho_{130} ($^{\mathrm{FITC}}$*Vc*Rho_{130}) on addition of *Vc*YaeO. Fig. 3d shows the progressive quenching of FITC fluorescence of $^{\mathrm{FITC}}$*Vc*Rho_{130} with increasing amounts of *Vc*YaeO, indicating the formation of a complex. The binding affinity (K_{d}) calculated from this reaction is 2.7 ± 0.3 μM (Fig. 3e and Table 3). Binding affinity between *Vc*Rho_{130} and *Vc*YaeO (dimer) was also estimated by isothermal titration calorimetry (ITC) that produced a K_{d} value of 7.63 ± 1.4 μM and stoichiometry of 1:1, with

Table 2. Structural homolog of *Vc*YaeO and their various parameters.

Molecule name	PDB ID	Number of residues (align/total)	% Identity	*Z*-score	RMSD
Salmonella typhimurium HFQ	2YLC	64/66	13	9.6	2.2
Escherichia coli HFQ	4PNO	62/64	13	9.2	2.1
Staphylococcus aureus HFQ	1KQ2	60/62	13	9.0	1.8
Methanococcus Jannaschii uncharacterized protein HFQ like	5DY9	56/56	16	8.8	2.0
Mycobacterium smegmatis ribosomal protein (ribosome maturation factor RIMP)	5GL6	59/169	8	7.4	2.7
Xenopus laevis small nuclear ribonucleoprotein F	4F7U	60/74	13	7.4	2.2
Homo sapiens gem-associated protein 6	1Y96	61/86	15	7.2	2.6
E. coli YaeO	1SG5	67/86	24	4.5	3.5

favorable values of entropy and enthalpy changes (Fig. 3f and Table 4).

Inhibition of Rho function and its manifestation

To see whether this binding has any influence on the function of the Rho protein, we have determined the RNA-dependent ATPase activity of *Vc*Rho in presence and absence of *Vc*YaeO by malachite green method [18]. The ATPase activity of the *Vc*Rho decreases sharply in presence of *Vc*YaeO as evident from their kinetic parameters (Fig. 4a and Table 5).

*Ec*Rho and *Vc*Rho proteins have 91% sequence identity (similarity 97.3%; Supplementary Fig. S4). Homology model of *Vc*Rho, as expected, is very

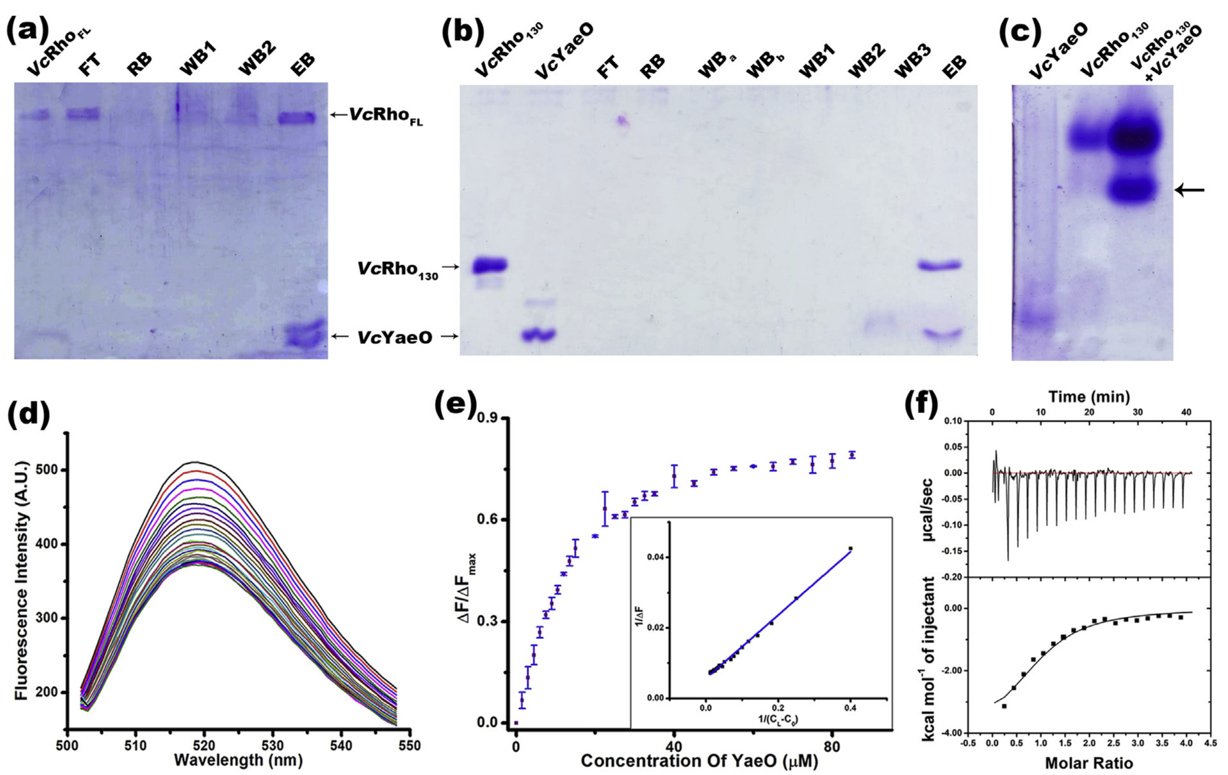

Fig. 3. Interaction of *Vc*YaeO with *Vc*Rho. (a) Pull-down experiment of His-tagged *Vc*Rho$_{FL}$ with *Vc*YaeO (non-His) where lanes from left to right contains His-tag *Vc*Rho$_{FL,}$ flowthrough (FT), and fractions eluted after washing with reaction buffer (RB), wash buffer 1 (WB1), wash buffer 2 (WB2), and elution buffer (EB). (b) Pull down of His-tag-*Vc*Rho$_{130}$ with *Vc*YaeO (non-His) where lanes from left to right contains His-tag-*Vc*Rho$_{130}$, *Vc*YaeO, FT, and fractions eluted after washing with RB, WB$_a$, WB$_b$, WB1, WB2, WB3, and EB. (c) Native gel showing the position of *Vc*YaeO (lane 1) *Vc*Rho$_{130}$ (lane 2) and the band for *Vc*Rho$_{130}$:*Vc*YaeO complex (marked by arrow; lane 3). (d) Emission spectra of FITC labeled *Vc*Rho$_{130}$ in the presence of increasing concentration of *Vc*YaeO at 293 K. (e) The binding isotherm obtained from steady-state fluorescence spectroscopy, with a double reciprocal plot in the inset. K_d value has been reported in Table 3. (f) Isothermal titration calorimetry (ITC) of *Vc*Rho$_{130}$ titrated with *Vc*YaeO at 293 K; the thermodynamic parameter has been reported in Table 4.

Table 3. Dissociation constant (K_d) values of *Vc*YaeO with different substrates derived from fluorescence quenching studies.

Protein − substrate	K_d (μM)
*Vc*YaeO − *Vc*Rho_{130}	2.71 ± 0.23
*Vc*YaeO − GTP	25.23 ± 1.85
*Vc*YaeO − CTP	30.58 ± 3.82
*Vc*YaeO − dG_{12} (ssDNA)	7.87 ± 0.65
*Vc*YaeO − dC_{12} (ssDNA)	7.42 ± 0.54
*Vc*YaeO − rG_{12} (RNA)	3.71 ± 0.23
*Vc*YaeO − rC_{12} (RNA)	4.97 ± 0.67

similar to *Ec*Rho, which indicated that dissimilar residues are located away from the primary RNA−binding site (PBS) and the hexameric interface (Supplementary Fig. S4). Therefore, *Vc*YaeO is likely to interact with *Ec*Rho and would inhibit the RNA-dependent ATPase activity of the latter. We have demonstrated through TLC method (see Materials and methods) that in presence of *Vc*YaeO, the rate of ATP hydrolysis decreases to 1/3 (Fig. 4b). Therefore, it is likely that *Vc*YaeO would inhibit the functions of *Ec*Rho *in vivo,* which would be manifested by the lethality of the strains because Rho is an essential protein. We overexpressed *Vc*YaeO in *E. coli* BL21 strain using various concentrations of isopropyl-*d*-1-thiogalactopyranoside (IPTG) to check the lethality (Fig. 4c−f). We observed that the expression of *Vc*YaeO in the presence of ≥50 μM IPTG induced lethality to the cells (Fig. 4e and f). This lethality was not observed either when the strain was transformed with an empty vector (pET28) or when an unrelated protein *Vc*AcP was overexpressed (Fig. 4c−f). These results indicated that *Vc*YaeO could specifically and efficiently inhibit transcription termination by *Ec*Rho *in vivo*, thereby affecting the cell viability.

*Vc*YaeO disrupts the hexameric assembly of *Vc*Rho

The aforementioned results clearly showed that *Vc*YaeO is structurally different from the *Ec*YaeO, but both of them inhibit Rho functions. Therefore, the mode of inhibition by *Vc*YaeO is expected to be significantly different from that of the *Ec*YaeO. To explore this, we checked the oligomeric states of the *Vc*Rho in the presence of YaeO by monitoring the elution profiles of the *Vc*Rho from a superdex 200 increase column, in the presence and absence of *Vc*YaeO. In the presence of an ATP analog, AMPPNP, *Vc*Rho_{FL} elutes as a single peak corresponding to a hexameric species having a molecular mass of 318 kDa (Fig. 5a−b). When different molar ratios (1:1, 1:2, 1:3; Rho monomer:YaeO dimer) of *Vc*YaeO were added to the *Vc*Rho + AMPPNP, the latter eluted as a species having molecular weight of ~70 kD (peaks 2, 3, and 5, in Fig. 5a and c). The *Vc*YaeO peaks were visible as peaks 4 and 6 (Fig. 5a and d). Analysis of peaks 2, 3, and 5 in SDS-PAGE showed two bands; one matched with *Vc*Rho_{FL}, while the other with *Vc*YaeO (Fig. 5e). Coelution of *Vc*Rho (46.7 kDa) with *Vc*YaeO (9.3 kDa) from a single peak not only demonstrates binding and complexation between these two proteins but quite interestingly it also suggests that binding of *Vc*YaeO to *Vc*Rho disrupts the hexameric integrity of *Vc*Rho required for its function. To ensure that the disruption of hexameric assembly of *Vc*Rho is not a dilution artifact, a control experiment with a mixture of *Vc*Rho in the presence of only buffer was performed, where *Vc*Rho_{FL} eluted as a hexamer (data not shown).

The oligomeric state of *Vc*Rho, either in presence or in the absence of *Vc*YaeO, was also tested by limited chemical cross-linking followed by SDS-PAGE (Supplementary Fig. S5). It showed the presence of hexameric form of *Vc*Rho in the absence of *Vc*YaeO, whereas in its presence, monomeric form of *Vc*Rho predominated.

To further confirm the oligomeric state(s) of the *Vc*Rho both in the absence and presence of the *Vc*YaeO, we measured the particle sizes of these species by DLS. The DLS experiments were performed at 20 °C and in the same buffer to match the conditions used in SEC. The measured hydrodynamic radius of free *Vc*Rho_{FL} and *Vc*Rho_{FL} bound to 5 mM ATP was 9.0 ± 0.8 nm and 8.7 ± 0.7 nm, respectively (Fig. 6a). But when *Vc*Rho_{FL} was mixed with *Vc*YaeO with a molar ratio of 1:2 (Rho monomer:YaeO dimer), in the absence and presence of 5 mM ATP, this radius reduced to 5.3 ± 0.6 nm and 5.6 ± 0.5 nm, respectively (Fig. 6a). So in the presence of *Vc*YaeO, hexameric assembly of *Vc*Rho_{FL} is disrupted, which further reinforces the proposition made in the previous paragraph. The ratio 1:2 of Rho monomer:YaeO dimer that disrupts hexameric assembly of *Vc*Rho_{FL} was ascertained in a separate experiment (Fig. 6b). The disruption of hexameric assembly started when

Table 4. Thermodynamics parameters obtained from calorimetric titration of *Vc*YaeO with *Vc*Rho_{130}, rG_{12} and rC_{12}.[a]

	Stoichiometry (N)	Dissociation constant (K_d) (μM)	Enthalpy (Δ*H*) (cal•mol^{-1})	Entropy (Δ*S*) (cal•mol^{-1}•deg^{-1})
VcRho_{130}	1	7.63 ± 0.78	−4.52E3 ± 0.6	9.4 ± 1.2
rG_{12} (RNA)	6	6.14 ± 0.85[b]	−1.92E5 ± 3.5E4[b]	−333 ± 38[b]
rC_{12} (RNA)	6	8.34 ± 1.5[b]	−4.2E4 ± 4.8E3[b]	160 ± 25[b]

[a] These are the average values for 6 consecutive sequential binding.
[b] All data are average of three independent measurements ± SD.

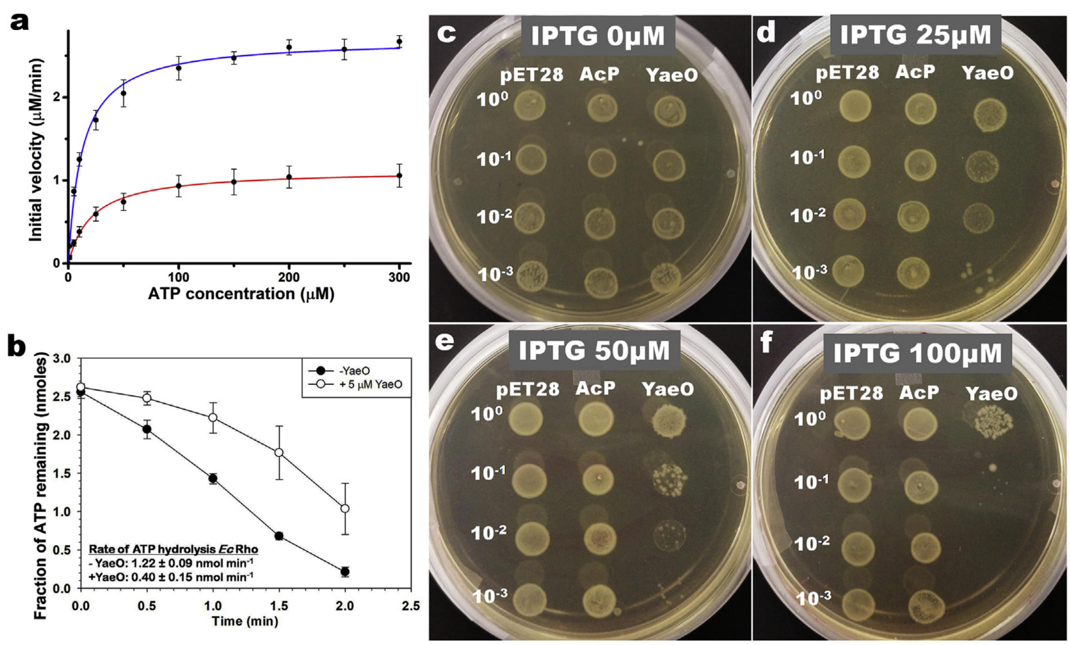

Fig. 4. ATPase activity of Rho and cell viability assays. (a) Steady-state kinetics of the RNA-dependent ATPase activity of *Vc*Rho in the absence (blue) and presence (red) of *Vc*YaeO measured by malachite green method. kinetic parameters listed in Table 5 (b) RNA-dependent ATP hydrolysis of *Ec*Rho measured in presence and absence of *Vc*YaeO by TLC method. (c–f) Cell viability assay of *Escherichia coli* BL21 (DE3) cells containing empty pET28a+, *Vc*AcP, and *Vc*YaeO. Overnight culture for each transformed cells and their three serial dilutions, as indicated, were spotted on kan plate. Plates were induced with varying amount of IPTG (0–100 μM). Lethality to the cells is evident with the overexpression of *Vc*YaeO containing ≥50 μM IPTG (e), whereas lethality was not observed either when the strain transformed with an empty vector (pET28) or when an unrelated protein *Vc*AcP was overexpressed (c–f).

the molar ratio of *Vc*Rho:*Vc*YaeO reached 1:1 (Rho monomer:YaeO dimer), and it completed at molar ratio of 1:2 (Rho monomer:YaeO dimer) (Fig. 6b). However, when *Vc*YaeO was added in the presence of ATP and poly (dC_{34}) (ssDNA with 34 cytosine bases), the disruption of hexameric conformation was not observed (Fig. 6c).

Hence, we concluded that *Vc*YaeO inhibits *Vc*Rho activities by disrupting the oligomeric states when the PBS of the *Vc*Rho is not occupied by the RNA or ssDNA. It is also possible that the presence of ssDNA or RNA in the PBS outcompetes *Vc*YaeO. These results further indicated that *Vc*YaeO inhibits Rho in a mechanism different from that of *Ec*YaeO [10].

Interaction of *Vc*YaeO with nucleotides

Although both *Vc*YaeO and *Ec*YaeO are close structural homologs of Hfq, *Ec*YaeO does not interact with single-stranded DNA [10]. Our structural and phylogenetic analyses on *Vc*YaeO revealed more resemblance with Hfq proteins than *Ec*YaeO (Table 2), indicating *Vc*YaeO might bind with single-stranded DNA. The superposition of *Vc*YaeO structure to that of the nucleotide and RNA-bound Hfq revealed that the RNA-binding site of the latter matches with *Vc*YaeO, which is populated with a tryptophan and two tyrosine residues (Fig. 7a). Therefore, if these aromatic amino acids define the ssDNA- or nucleotide-binding sites, the nucleic acid–binding properties of *Vc*YaeO could be measured by fluorescence quenching techniques. Among the four nucleotides, CTP and GTP have been observed to quench the tryptophan fluorescence of *Vc*YaeO indicating their specific binding (Table 3, Fig. 7b).

As this protein binds to C and G, we next checked its binding with different C- and G-rich single-stranded DNA and RNA oligos, dC_{12}, rC_{12}, dG_{12}, and rG_{12} using the intrinsic tryptophan fluorescence of *Vc*YaeO. The progressive tryptophan fluorescence quenching of *Vc*YaeO with the increasing concentrations of these oligos suggested their specific binding. Binding constants calculated from fluorescence quenching data (Fig. 7c–f and Table 3) is in agreement with our speculation. The binding

Table 5. Steady-state kinetic parameters for the RNA-dependent ATPase activity of $VcRho_{FL}$.

ATPase activity	K_m (μM)	V_{max} (μM min^{-1})	k_{cat} (min^{-1})
$VcRho_{FL}$	12.0 ± 1.05	2.6 ± 0.12	10.5 ± 0.48
$VcRho_{FL}$ + *Vc*YaeO	19.5 ± 2.43	1.09 ± 0.15	4.4 ± 0.6

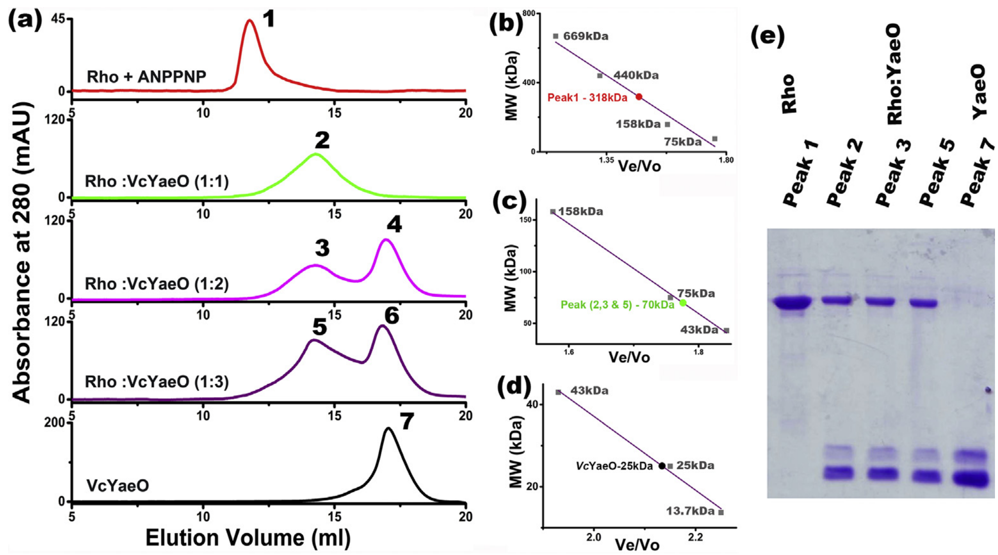

Fig. 5. Size exclusion chromatography of *Vc*Rho. *Vc*Rho_{FL} in presence of AMPPNP eluted mostly as hexamer (peak 1 in red). However, in presence of *Vc*YaeO with molar ratio greater than 1:1 (monomer:dimer), its hexameric form disrupts to lower oligomeric form as evident in peaks 2, 3, and 5 (green, magenta, and violet colored elution profile). Molecular weights calculated from standard curves are (b)*Vc*Rho_{FL} ≈ 318 kDa, (c) *Vc*Rho_{FL} and *Vc*YaeO complex ≈ 70 kDa, and (d) *Vc*YaeO, Mw ≈ 25 kDa (considering dimer). (e) SDS-PAGE analysis demonstrates the presence of both *Vc*Rho_{FL} and *Vc*YaeO in peaks 2, 3, and 5, which indicates the formation of a complex between them.

affinity and stoichiometry of *Vc*YaeO−rG_{12} and *Vc*YaeO−rC_{12} interactions were also determined by ITC (Fig. 7g and h and Table 4). *Vc*YaeO binds sequentially with rG_{12} and rC_{12} with a stoichiometry (6:1); the average K_d values are 6.14 ± 1.1 μM and 8.34 ± 1.4 μM, respectively.

Hfq protein from *Pseudomonas aeruginosa* can bind to three nucleotides (UTP, CTP, and ATP) [16], whereas *Vc*YaeO binds only two of them (GTP and CTP) close to the site of W56 residue. The binding affinity of Hfq proteins toward specific RNA sequences (regions of ropS and DsrA) is in the few nanomolar (nM) range [19], but for nonpreferred sequences, this value decreases to 390 nM (for rA_7) [19] or 14.9 μM (for rG_6) [20]. In case of *Vc*YaeO, the affinity for rG_{12} and rC_{12} is about 4 μM, which is comparable with the nonspecific binding affinity of Hfq. *Vc*YaeO might have specific RNA sequences to which it binds more tightly.

Structural model of *Vc*Rho and *Vc*YaeO complex and probable mechanism of Rho-hexamer dissociation

To get further insight into the mechanism of inhibition of Rho by *Vc*YaeO, we constructed a structural model of *Vc*YaeO:*Vc*Rho complex. A negatively charged patch comprising of D5, E52, D13, D14, D16, D44, E57, E61, and E64 is observed on the surface of *Ec*YaeO [10], out of which D5, D44, E52, E57, and E64 have been observed to interact with the positively charged residues located at the PBS of Rho [10]. *Ec*YaeO:*Ec*Rho complex formation is therefore governed by salt bridge/ionic interactions, which is consistent with the pull-down assays reported earlier [9,10]. All these acidic residues are not conserved in other YaeOs (Fig. 1a), rather a subset of these residues covering the middle of the patch is conserved (Fig. 1a). This implies that these residues contribute to the core of the interactions, while interactions made in other places are peripheral and might be case specific. A comparison of the surface charges of *Ec*YaeO and *Vc*YaeO is shown in Fig. 8a, where different orientations of their N-terminus loop and charge equivalence of Rho interacting residues are shown. We constructed a docked model between *Vc*YaeO and the homology model of *Vc*Rho based on the *Ec*YaeO:*Ec*Rho complex and multiple sequence alignments (Fig. 1). Because *Vc*YaeO exists as dimer in solution, we also fitted the *Vc*YaeO dimer with our current model avoiding any steric clash, both with the open- (Supplementary Fig. S6) and closed-ring structure (Fig. 8b). Analysis of *Vc*YaeO dimer indicates that N-terminal helix residues have low B-factors, and this helix is involved in dimerization. Moreover different orientation of the N-terminal helix, in *Ec*YaeO *or* *Vc*YaeO, is synchronized with the altered length/orientation of β5−β6 loop (Fig. 2c). Therefore, it is unlikely that N-terminal helix would assume different orientation relative to the core by breaking its interactions with β5−β6 loop and the dimeric interface. However, by compromising these interactions, if we consider the orientation of N-

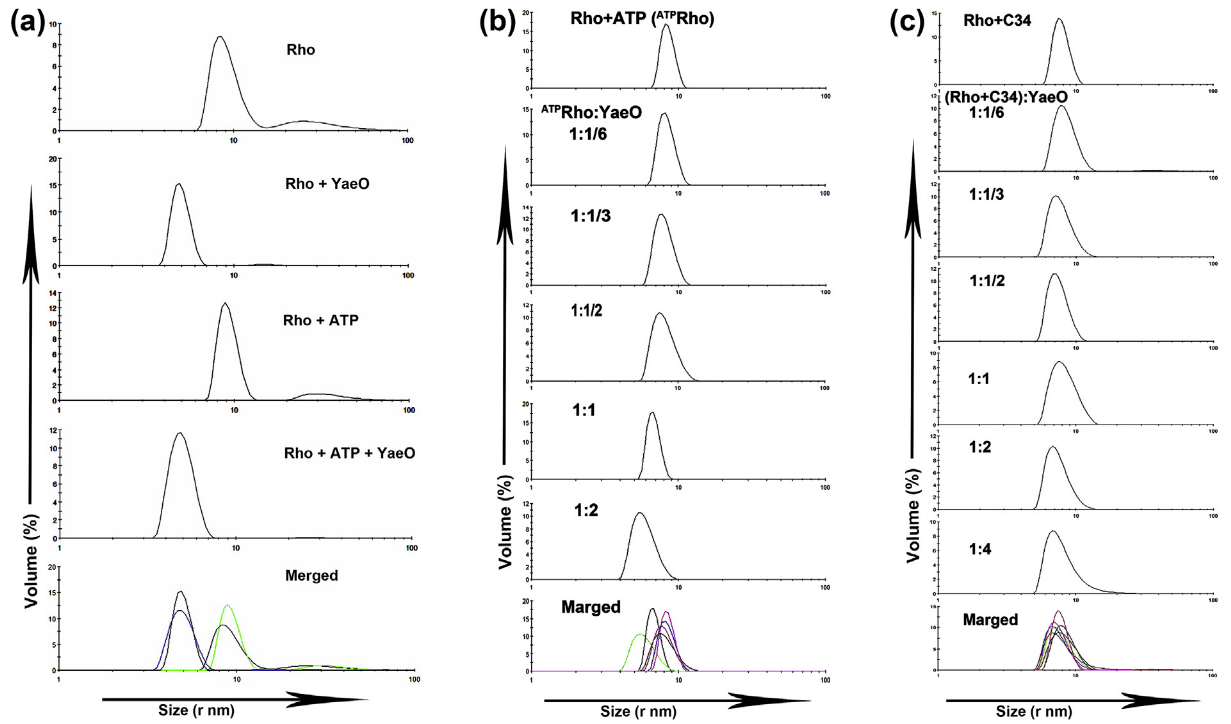

Fig. 6. Disruption of hexameric assembly of *Vc*Rho by *Vc*YaeO through DLS. Particle size in terms of volume distribution. (a) *Vc*Rho exhibits a mean hydrodynamic radius (R_h) of 9.0 $\pm$ 0.8 nm, whereas in presence of *Vc*YaeO, *Vc*Rho showed an R_h of 4.8 $\pm$ 0.5 nm. In presence of only ATP or ATP + *Vc*YaeO, *Vc*Rho showed R_h value of 8.7 $\pm$ 0.7 nm and 5.0 $\pm$ 0.6 nm, respectively. Superposition of all the four distribution—green and black on the right is for *Vc*Rho in the absence and presence of ATP and blue and black on left for *Vc*Rho + *Vc*YaeO in the absence and presence of ATP. Disruption of hexameric form of *Vc*Rho in presence *Vc*YaeO is evident. (b) DLS profiles of *Vc*Rho-ATP with increasing molar ratio of *Vc*YaeO indicates that dissociation of Rho-hexamer started when the molar ratio reached 1:1 (Rho monomer:YaeO dimer) and it completed at molar ratio of 1:2. (c) *Vc*Rho-ATP-$(dC)_{34}$ DLS profiles with increasing molar ratio of *Vc*YaeO shows no noticeable change in particle size.

terminal helix to be like *Ec*YaeO, we do not find any steric clashes with the neighboring Rho subunit. This *Vc*YaeO:*Vc*Rho model (Fig. 8b) was subjected to molecular dynamics (MD) simulations, and the complex is seen to be stable over 650 ns (Fig. 8c). The structure revealed that one monomer occupies the PBS of *Vc*Rho, whereas the β5−β6 loop of the second monomer interacts with the connecting loops of the NTD and CTD of Rho (Fig. 8d). In the complex, *Vc*YaeO appeared to block the PBS of the *Vc*Rho, and hence, it could compete with the RNA binding at the PBS (Fig. 8d).

As mentioned earlier, homology model of *Vc*Rho is structurally very similar to *Ec*Rho, and their dissimilar residues are located away from the PBS and the hexameric interface. In the *Vc*YaeO:*Vc*Rho model, D36(D44)−K100, D36(D44)−R102, E45(E52)−R88 (residues within bracket are *Ec*YaeO residues) interactions are preserved, whereas E57−K102 and E64−K105 interactions seen in *Ec*YaeO:*Ec*Rho are lost as the corresponding residue in *Vc*YaeO are basic and hydrophobic. Interestingly, new ionic interactions are gained in this complex involving residues E11−K115, E11−R88, N38−R102, N39−E108, K43−D60, and E45−R88 (Fig. 8e). Although this model does not explain the mechanism of hexameric dissociation by *Vc*YaeO, we speculate that its unique β5−β6 loop could perturb the linker conformations between the N- and C-terminal domains of Rho.

Discussion

Rho is unique to prokaryotes and essential for cell viability of many bacterial species; as a consequence, it is an attractive target for drug development. Among the Rho inhibitory proteins, Psu and YaeO, the structure and mechanism of Psu have been described earlier by our group [7,8]. Here, we functionally and structurally characterize YaeO protein from the pathogen, *V. cholerae*. Although a tight binding between *Ec*Rho and *Ec*YaeO has been demonstrated before [10], the exact nature of the YaeO-induced antitermination is unknown. Our structural, bioinformatic, and phylogenetic analyses

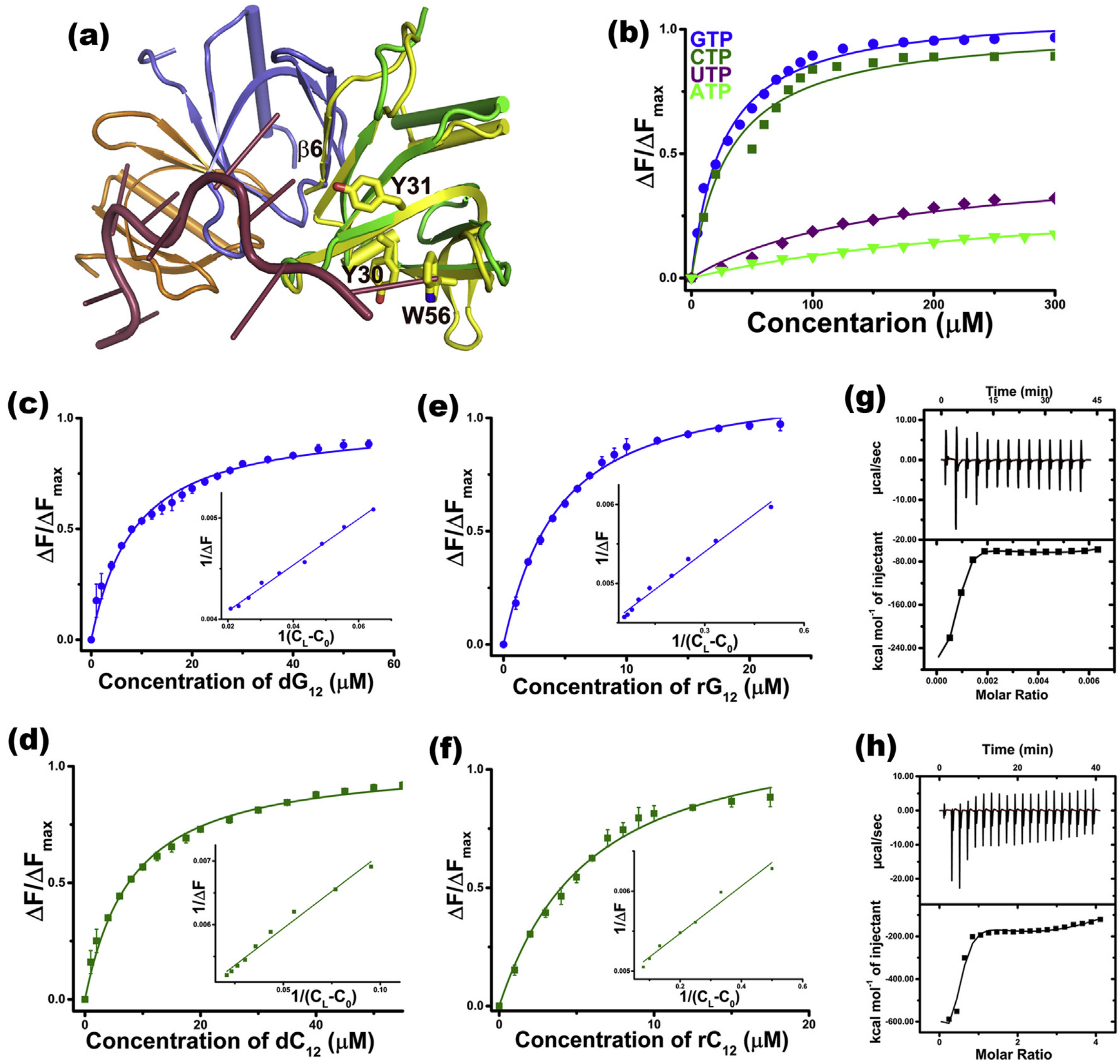

Fig. 7. The interaction of *Vc*YaeO with G & C oligonucleotides. (a) Superposition of the structure of *Vc*YaeO (yellow) on RNA bound *E. coli* Hfq (PDB ID: 3GIB) is showing that W56, Y30 and Y31 of *Vc*YaeO is close to the location of the first base (raspberry cartoon). (b) Binding isotherms obtained from steady-state fluorescence spectroscopy of *Vc*YaeO with four nucleotides are indicated. Binding isotherm and double reciprocal plot (inset) of *Vc*YaeO and single-stranded DNA/RNA dG_{12} (c), dC_{12} (d), rG_{12} (e), and rC_{12} (f) are represented. All K_d values are represented in Table 3. Binding of *Vc*YaeO titrated to rG_{12} (g) and rC_{12} (h) was assayed by ITC at 20 °C. The thermodynamic parameters have been reported in Table 4.

demonstrated that *V. cholerae* YaeO is distinctly different from *Ec*YaeO. *Vc*YaeO structurally resembles with Hfq protein that is consistent with the unique ssDNA/RNA-binding properties of *Vc*YaeO (Fig. 7). In spite of the dissimilarities with *Ec*YaeO, *Vc*YaeO binds to *Vc*Rho and inhibits its function. However, the *Vc*YaeO exerts this inhibition by disrupting the oligomeric structure of *Vc*Rho (Figs. 5 and 6), which is a unique and novel mechanism and never been reported for any other Rho inhibitor.

*Vc*YaeO has only 24% sequence identity with *Ec*YaeO, and our phylogenetic analysis indeed revealed that *Vc*YaeO-type proteins are distinctly different from *Ec*YaeO-type proteins (Fig. 1a and c). Multiple sequence alignment of YaeO-type proteins indicates conservation of only few residues throughout the family (Fig. 1a). Surface-exposed nature of these residues points toward their possible involvement in biological function. High degree of structural differences in the surface-exposed loops β1−β2, β2−β3, β4−β5, and β5−β6, different orientation of α1 (Fig. 2c and d), and low sequence identity render distinct surface charge and grooves of *Vc*YaeO as compared with *Ec*YaeO. It implies that *Vc*YaeO might exhibit different modes of interactions with

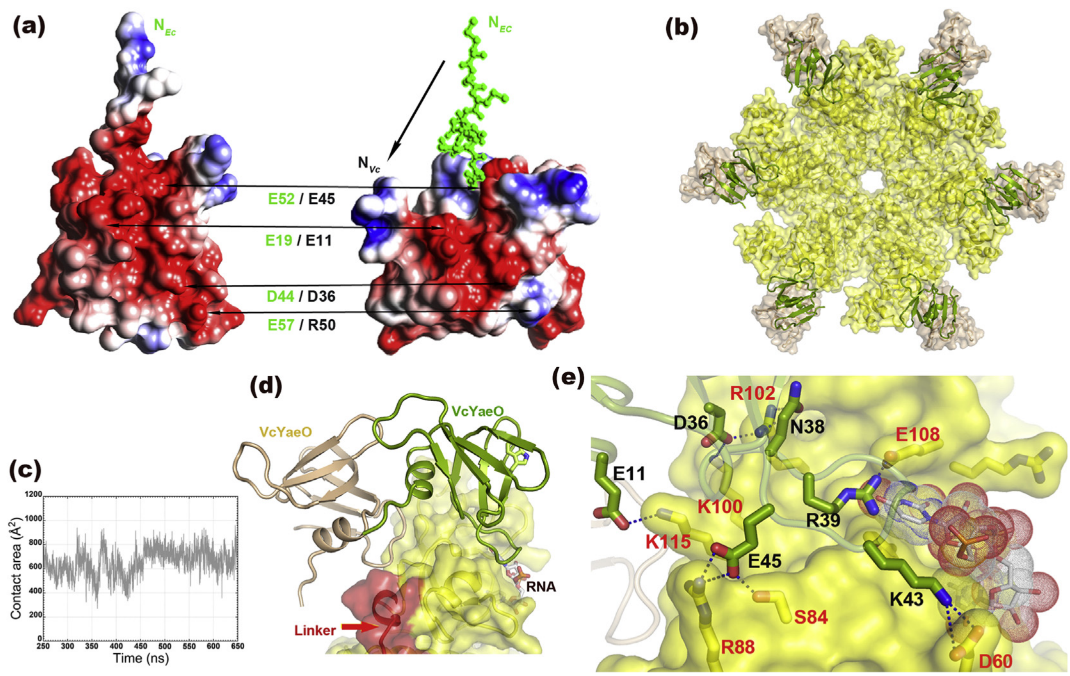

Fig. 8. Modeling *Vc*YaeO and *Vc*Rho interaction. (a) Electrostatic charge surface of *Ec*YaeO (left) and *Vc*YaeO (right). Residues implicated in Rho binding in *Ec*YaeO and their equivalences in *Vc*YaeO are indicated. Different orientation of the N-terminus loop of *Ec*YaeO (in sticks) with respect to *Vc*YaeO is indicated by an arrow (right). (b) Model of *Vc*YaeO dimer (green cartoon and flesh surface) bound with *Vc*Rho (yellow surface) hexamer. (c) Buried surface area between *Vc*YaeO (dimer) and Rho, which is stable during the last 400 ns MD simulations. (d) Zoomed view of the orientation of *Vc*YaeO dimer and *Vc*Rho showing one monomer (green) blocks the RNA (sticks)-binding site, whereas other monomer (flesh) interacts with the linker/ATP-binding loop (red). (e) Probable interactions between *Vc*YaeO (green) with *Vc*Rho (yellow).

*Vc*Rho. Upholding of size and hydrophobic nature of the residues residing in β-sandwich core (Fig. 2b), on the other hand, signifies their role in maintaining the fold integrity.

The results of different orthogonal techniques such as pull down, native page, fluorescence, and ITC proved that *Vc*YaeO has strong interaction with the N-terminal part of the *Vc*Rho (Fig. 3). The *Vc*YaeO:*Vc*Rho interaction, proposed from our modeling studies, indicates that the interaction is predominantly ionic, but the set of residues engaged during this process is quite different from the *Ec*YaeO protein. Amino acid sequences of *Vc*Rho and *Ec*Rho differ at several places, but none of them reinforce the *Vc*YaeO interaction site (Fig. S4). Therefore, *Vc*YaeO would be capable to inhibit *Ec*Rho in a similar manner. Decreasing cell viability of *E. coli* with increased expression of *Vc*YaeO indeed shows similar transcription termination inhibition *in vivo* (Fig. 4d–f).

Although both of *Vc*YaeO and *Ec*YaeO bear close structural similarities with Hfq, unlike *Vc*YaeO, *Ec*YaeO shows no detectable interaction with single-stranded DNA [10]. This is not surprising because resemblance with Hfq-type protein is more with *Vc*YaeO than that with *Ec*YaeO (Table 2). It can be envisaged as an additional Hfq-like property of *Vc*YaeO. The ssDNA/RNA-binding site in *Vc*YaeO has been identified near the W56 located close to the β2–β3 loop. Incidentally, our modeling study has shown that this loop of *Vc*YaeO hinders the interactions in PBS of Rho. We propose that *Vc*YaeO on binding to Rho could compete with Rho-PBS for the same ssDNA/RNA.

In the presence of ATP, Rho remains in homohexameric form, which is likely the intercellular oligomeric form essential for its function. One of the intriguing facts emerged from our studies is that *Vc*YaeO has the ability to disrupt the hexameric assembly of *Vc*Rho. Because the very hexameric structure of Rho required for its function is lost, the process of transcription termination would be abrogated. How does *Vc*YaeO disrupt the Rho oligomeric structure? Although we do not have the exact explanation for this process, it is tempting to propose that by virtue of ssDNA/RNA-binding properties of *Vc*YaeO, it could pull out nucleic acids from the Rho PBS and thereby destabilize the oligomeric state(s). Rho cofactors play important roles to stabilize the oligomeric form of Rho [21], and their absence induces lower oligomeric states to Rho. In the modeled complex, one *Vc*YaeO subunit from the *Vc*YaeO dimer could directly access the PBS, whereas the other subunit interacts with RNA only through the filling residues. The unique β5−β6 loop of these subunits of YaeO could interact with the linker region connecting the N- and C-terminal domains of Rho, and it is also possible that it might affect the intrasubunit interactions of the latter, making *Vc*YaeO-mediated displacement of RNA from *Vc*Rho and disruption of the VcRho oligomer to occur simultaneously or within a short time interval.

Materials and Methods

Phylogenetic and multiple sequence alignment analysis

The sequence of *Vc*YaeO (81 residues; UniProt accession code: A0A0H3ADN9) was used as template for blast search in PRABI-GERLAND:RHONE-ALPES BIOINFORMATIC POLE GERLAND SITE at NPS@ server using the NR protein sequences database (UniProtKB 60% identity maximum + PDB sequences) with expectation value (−e, real) 100 in BLOSUM62 matrix. About 135 sequences were selected from the database with E threshold ≤ 1. Out of them, only 121 sequences were chosen with sequence length ≤ 130 and were used to generate phylogenetic tree in Multalin server. These sequences were analyzed and aligned by Multalin [22], which prepares the multiple sequence alignment with hierarchical clustering using the matrix blosum62, with gap weight −12 and gap length weight −2. Thirteen representative protein sequences have been selected from different genus to produce the multiple sequence alignment. The phylogenic tree was generated with a maximal number of clusters of 13 and minimal distance between sequences 10 PAM.

Cloning, expression, and purification of *Vc*YaeO, *Vc*Rho, and *Vc*Rho$_{130}$

The coding sequence of *Vc*YaeO (246 bp; 81 amino acids), *Vc*Rho$_{FL}$ (1260 bp and 419 amino acids), and N-terminal domain of *Vc*Rho (first 130 amino acids, *Vc*Rho$_{130}$; 390 bp) was amplified by PCR from the genomic DNA of *V. cholerae* (strain O395) and cloned into the MCS of the expression vector pET28a+ (Novagen) using *Nde*I (forward) and *Bam*HI (reverse) restriction sites. The clones were transformed into BL21 (DE3) cell, and overexpression of the proteins was checked following the protocol described in NEB. Amount of IPTG used for induction was optimized as 400 μM, 200 μM, and 300 μM for *Vc*YaeO, *Vc*Rho$_{FL}$, and *Vc*Rho$_{130}$, respectively.

To get purified protein, 15 ml of LB media was inoculated with BL21 (DE3) cell (containing the desired clone) from glycerol stock and grown overnight at 310 K. 1 l LB broth was inoculated with 15 ml of the overnight culture, and the culture was grown at 310 K until the OD_{600} reached 0.6. The cells were then induced with the respective amount of IPTG. After overnight incubation at 293 K, cells were harvested by centrifugation at 4000 RCF for 10 min at 277 K. The pellet was resuspended in required amount of ice-cold lysis buffer (50 mM Tris−HCl pH 8.0, 300 mM NaCl, 2 mM phenylmethanesulfonyl fluoride, 2 mM dithiothreitol [DTT]). The cells were lysed by the addition of lysozyme followed by sonication. The cell lysate was then centrifuged at 13000 RCF for 45 min. The supernatant was applied onto a nickel−nitrilotriacetic acid affinity chromatography media (Qiagen) that was previously equilibrated with buffer-A (50 mM Tris−HCl pH 8.0, 300 mM NaCl, 2 mM DTT). The protein was eluted with 300 mM imidazole in buffer A. The 6 × His tag was cleaved using restriction-grade thrombin (Novagen), and the final purified protein was achieved by gel filtration using a Superdex-200 (GE Healthcare) column preequilibrated with buffer B (50 mM Tris−HCl pH 8.0, 300 mM NaCl, 0.5 mM DTT). The purified proteins were used for crystallization, biophysical, or biochemical assay, except *Vc*YaeO, which was treated with iodoacetamide/TCEP hydrochloride (five times the protein concentration) to avoid precipitation. The homogeneity of the purified protein was determined by SDS-PAGE using 12% or 15% polyacrylamide gel as required.

Crystallization and data collection

*Vc*YaeO was concentrated to 15 mg ml^{-1} in a buffer containing 50 mM HEPES (pH 7.0), 200 mM NaCl using an Amicon Ultra centrifugation unit (molecular weight cutoff 3 kDa). The concentration of the protein was measured spectrophotometrically using a calculated extinction coefficient of 11,460 M^{-1} cm^{-1}. Initial crystallization trials were performed by the hanging-drop vapor diffusion methods in 24-well crystallization trays (Hampton Research, Laguna Niguel, California, USA) using the precipitants of Grid Screen PEG 6000, Grid Screen Ammonium Sulfate, Crystal Screen, and Crystal Screen 2 from Hampton Research [23]. 2 μl of protein solution was mixed with 2 μl of precipitant solution, inverted over a reservoir containing 600 μl precipitant solution, and maintained at both 277 and 293 K. Crystallization setup with iodoacetamide-treated protein finally produced diffraction quality crystals.

Crystals were looped out from the crystallization drops using a 20 μm nylon loop and briefly soaked in crystallization solution containing 30% (v/v) glycerol as cryoprotectant and flash-cooled in liquid nitrogen (Oxford Cryosystems) at 100 K. X-ray diffraction data were collected on PX BL-21 beamline of Indus-2 synchrotron at RRCAT, Indore (wavelength 0.979 Å) [24], to a resolution of 1.75 Å using MARCCD 225 (rayonix) detector with a distance of 190 mm. A total of 315 frames were recorded with an oscillation of 1°. The data were indexed, integrated, and scaled with the XDS package [25], and the details of the data collection and processing statistics are given in Table 4. Calculations of Matthews coefficient [26], using CCP4 Program Suite 6.4.0 [27], indicated the presence of two molecules of *Vc*YaeO in the asymmetric unit with a solvent content of 66%.

Structure determination and refinement

A BLAST search of *Vc*YaeO sequence against PDB did not identify any crystal structure having appreciable sequence identity. The most prominent result found in the BLAST search is the NMR structure of *Ec*YaeO with a moderate identity (24%). However, MR calculations performed with the 20 models of *Ec*YaeO (PDB code: 1SG5) failed to produce any definite solution. Attempt to solve the structure using the core secondary structure of *Ec*YaeO, where the flexible loops were deleted, failed either. Next, structural homologs of *Ec*YaeO, identified through DALI server, were used for MR calculations. Several structures with high (>3) Z-score were identified, but their sequence identity is very low (~12%). These include translational regulator Hfq, archaeal Sm protein (1I8F), and small nuclear ribonucleoprotein sm d3 fragment (1D3B). MR calculations [28], with these models truncated to polyserine, showed that RNA-binding proteins Hfq (4PNO) produced best solution. The structure was improved by few cycles of model fitting in Coot [29] and refinement with phenix.refine [28]. This improved structure was subjected to the Autobuild module of phenix. High-resolution diffraction data allowed building most of the side chains with an R-factor of 22.4% (Rfree 25.8%). Three–four cycles of manual model corrections, TLS refinement, and water picking yielded the final model with good statistics (Table 4). The coordinates have been submitted with PDB code: 6JIE.

Structural analysis

PISA web server [17] was used for the analysis of oligomeric state. Figures were produced using Pymol (http://www.pymol.org) and surface electrostatic potential were calculated by Chimera [30]. DALI web server [14] was used to search structural homologs. Model building was done with Coot [29], and sequence analysis was done by Multalin server [22].

Pull-down assay of *Vc*YaeO and *Vc*Rho

For these assays, 50 μg of the His-tagged $Vc\mathrm{Rho}_{FL}$ and 10 μg of *Vc*YaeO (without His-tag) were mixed in 100 μl of reaction buffer (RB: 50 mM Tris–HCl pH 8.0, 200 mM NaCl) and incubated at 20 °C for 10 min. This $Vc\mathrm{Rho}_{FL}$ and *Vc*YaeO mixture was then added to 100 μl of Ni-NTA beads preequilibrated with the RB and incubated at room temperature for 10 min. The supernatant was kept as flowthrough after spinning at 2000 rpm for 2 min. The beads were then serially washed with 100 μl of RB, WB1 (50 mM Tris–HCl pH 8.0, 200 mM NaCl, 0.5 M KCl), and WB2 (50 mM Tris–HCl pH 8.0, 200 mM NaCl, and 50 mM imidazole). Finally, proteins bound to the beads were eluted with 100 μl of EB (EB; 50 mM Tris–HCl pH 8.0, 200 mM NaCl, and 300 mM imidazole).

To check the binding of *Vc*YaeO and $Vc\mathrm{Rho}_{130}$, 10 μg of His-tagged $Vc\mathrm{Rho}_{130}$ and 10 μg of non–His-tagged *Vc*YaeO were mixed in 100 μl of RB and incubated at 20 °C for 10 min. The mixture was added to 100 μl Ni-NTA beads preequilibrated with the RB and incubated at room temperature for 10 min. The supernatant was taken as flowthrough after spinning at 2000 rpm for 2 min. The beads were then washed with 100 μl of RB followed by washing with 100 μl WB_a (RB containing 200 mM KCl), 100 μl WB_b (RB containing 300 mM KCl), 100 μl of WB1, and 100 μl of WB2 and WB3 (WB3: 50 mM Tris–HCl pH 8.0, 200 mM NaCl, 100 mM imidazole). Finally, the proteins were eluted with 100 μl of EB.

Fluorescence quenching study for *Vc*YaeO and *Vc*Rho interaction

$Vc\mathrm{Rho}_{130}$ was covalently labeled with FITC (fluorescein derivative) in a buffer of pH ~9.0 (20 mM HEPES pH 7.5, 100 mM NaCl, 50 mM KCl and $NaHCO_3$). About 1 mg $Vc\mathrm{Rho}_{130}$ was reacted with 50-fold molar excess of FITC, taken in a small volume of dry acetone. The labeling was carried out in a buffer containing 20 mM $NaHCO_3$ for about 3 h at 4 °C. $^{FITC}Vc\mathrm{Rho}_{130}$ was separated and purified from the reaction mixture by gel filtration on a Sephadex G-10 column using the buffer containing 20 mM HEPES pH 7.5, 100 mM NaCl, and 50 mM KCl. The concentration of $^{FITC}Vc\mathrm{Rho}_{130}$ was determined using Lowry's method [31] and that of fluorescein was determined spectrophotometrically from the absorbance at 495 nm and using the molar extinction coefficient of 76,000 M^{-1} cm^{-1} [32]. The labeling ratio of fluorescein to $Vc\mathrm{Rho}_{130}$ in $^{FITC}Vc\mathrm{Rho}_{130}$ was 3:1.

The steady-state fluorescence measurements were performed using a VARIAN *Cary Eclipse* fluorescence spectrophotometer using 10-mm path length quartz cuvettes with 5-nm band-pass slits for both excitation and emission channels. 0.5 μM $^{FITC}Vc\mathrm{Rho}_{130}$ was excited at 495 nm, and the change in fluorescence emission intensity at 519 nm in the presence of increasing concentration of *Vc*YaeO was measured at 20 °C. K_d value of this interaction was determined using nonlinear curve fitting analysis as described previously [33] by using Equations (1) and (2). The fitting has been done by OriginPro 9.0 software package.

$$K_d = \{[C_0 - (\Delta F / \Delta F_{max}) \cdot C_0] \cdot [C_L - (\Delta F / \Delta F_{max}) \cdot C_0]\} / \{(\Delta F / \Delta F_{max}) \cdot C_0\} \quad (1)$$

$$C_0 \cdot (\Delta F/\Delta F_{max})^2 - [(C_0 + C_L + K_d) \cdot (\Delta F / \Delta F_{max})] + C_L = 0 \quad (2)$$

In equations (1) and (2), ΔF and ΔF_{max} are the change in fluorescence emission intensity and the maximum fluorescence intensity change. The concentration of ligands and the initial concentration of the protein are denoted by C_L and C_0. The ΔF_{max} was determined from a double reciprocal plot using the equation below.

$$1 / \Delta F = 1 / \Delta F_{max} + K_d / [\Delta F_{max}(C_L - C_0)] \quad (3)$$

Data are the mean of three independent experiments ± SD.

Gel filtration assay for *Vc*Rho and *Vc*YaeO interaction

SEC experiments were performed in a superdex 200 increase column (10/300) attached with an AKTApurifier (GE Healthcare life sciences). Before the experiment, VcRho_{FL} was incubated for 10 min in a buffer (25 mM HEPES pH 7.5, 100 mM NaCl, 50 mM KCl, 2% glycerol) containing 0.5 mM AMPPNP. $Vc\mathrm{Rho}_{FL}$ and *Vc*YaeO were mixed in different molar ratios, in presence of 0.5 mM AMPPNP and incubated for 10 min in the abovementioned buffer, after that, it was loaded to the SEC column to generate chromatograms. In each case, the column was preequilibrated with buffer (25 mM HEPES pH 7.5, 100 mM NaCl, 50 mM KCl, 2% glycerol, and 0.05 mM AMPPNP) and run with a flow rate of 0.5 ml/min. The column was calibrated by running thyroglobulin (669 kDa), ferritin (44 kDa), aldolase (158 kDa), conalbumin (75 kDa), ovalbumin (43 kDa), chymotrypsinogen A (26 kDa), and ribonuclease A (13.7 kDa) supplied by GE Healthcare life science.

ATPase assays

ATPase activity of purified *Vc*Rho_{FL} alone and *Vc*Rho_{FL} in presence of *Vc*YaeO was determined spectrophotomerically by measuring the release of inorganic phosphate (P_i) using the malachite green reagent, as described previously [18]. The molar ratio of *Vc*Rho_{FL}-Hexamer:*Vc*YaeO Dimer was 1:12 in the experiment. Briefly, the reactions were performed in 320 μl assays in 24-well microplates containing 50 mM Tris−HCl (pH 8.0), 100 mM NaCl, 100 mM KCl, 2 mM $MnCl_2$, 0−300 μM ATP (Sigma Aldrich), 1.5 μM poly(rC), and 0.25 μM of *Vc*Rho_{FL}-hexamer alone or 0.25 μM of *Vc*Rho_{FL}-hexamer in presence of 3 μM *Vc*YaeO-dimer. After 20 min incubation at 37 °C, the reaction was stopped by the addition of 80 μl of malachite green, and production of Pi was measured at 630 nm by Epoch BioTek plate reader. Kinetic parameters were determined by nonlinear curve fitting from the Michaelis−Menten plot using OriginPro 9.0. Data are the mean of three independent experiments ± SD.

Inhibition of ATPase activity of Rho proteins from *E. coli* by *V. cholerae* YaeO was determined as described previously [34]. Rho proteins (100 nM) premixed with or without YaeO (5 μM) were incubated at 37 °C for 10 min and then added to buffer (25 mM Tris−Cl pH 8.0, 50 mM KCl, 5 mM $MgCl_2$, 2 mM DTT, 0.1 mg/ml BSA, and 1 mM ATP). γ-^{32}P ATP (3500 Ci/mmol; BRIT, India) was added as tracer in the reaction mixture. After collecting an aliquot for the T_0, ATPase reaction was initiated by addition of 20 μM poly(rC) as RNA template. At different time points, aliquots were collected, and reaction was stopped with 1.5 M formic acid. The amount of ATP hydrolyzed at different time points was monitored by separating released P_i from ATP on a polyethylenimine TLC chromatography sheet (Merck KGaA, Darmstadt, Germany) with 0.75 M KH_2PO_4 pH 3.5 as mobile phase. After chromatographic separation, TLC sheets were exposed to phosphorimager screen and subsequently scanned with Typhoon FLA 9500 (GE Healthcare Bio-Sciences AB, Sweden). Percentage of ATP hydrolyzed was determined by the intensity of ATP remaining at different time points compared with the intensity of ATP at T_0 and was plotted against time. Data are the mean of three independent experiments ± SD.

Cell viability assay

Empty pET28a+ vector, *V. cholerae* acylphosphatase (*Vc*AcP, uniprot: A5F8G9; Mw 10.226 kDa) cloned in pET28a+ vector, and *Vc*YaeO cloned in vector pET28a+ have been transformed in to BL21(DE3). Each clone was separately inoculated in 5 ml LB media and cultured overnight. Each overnight culture was serially diluted (10^0, 10^{-1}, 10^{-2} and 10^{-3} folds) and spotted on plates containing 30 μg/ml kanamycin (resistivity gained by pET28a+). Different amount of IPTG (0 μM, 25 μM, 50 μM, 100 μM) were used for differential induction of gene cloned in pET28a+. After overnight incubation at 37 °C, plates were analyzed for viability.

Isothermal titration calorimetry

ITC experiments were carried out using an iTC 200 calorimeter (GE Healthcare Bio Sciences Ltd.). Calorimetric titrations of *Vc*Rho_{130} (2 μM in the cuvette) by *Vc*YaeO (40 μM in the syringe; 2 μl injections) were carried out at 20 °C in assay buffer (25 mM HEPES pH 7.5, 100 mM NaCl, 50 mM KCl) with a spacing of 120 s between injections (20 injections). Titrations of rG_{12} and rC_{12} (10 μM in the cuvette) by *Vc*YaeO (200 μM in the syringe; 3 μl injections for rG_{12}) and (300 μM in the syringe; 2 μl injections for rC_{12}) were carried out at 20 °C in assay buffer (25 mM HEPES pH 7.5, 50 mM NaCl, 50 mM KCl, 5 mM $MgCl_2$) with a spacing of 180 s for rG_{12} and 120 s for rC_{12} between injections (14 injections for rG_{12} and 20 injections for rC_{12}). ITC data were analyzed by integrating heat effects normalized to the amount of injected protein and curve-fitting based on a single-site binding model in case for *Vc*Rho_{130} and sequential binding model to 6 sites for rG_{12} and rC_{12}, using the Origin software package (ORIGIN MicroCal, OriginLab Corporation, Northampton, MA, USA) provided by the vendor. The dissociation constants were derived from the data by using standard procedures. The data used to calculate binding constants (K_d), Stoichiometry (N) and thermodynamic parameters [Enthalpy (ΔH) and Entropy (ΔS)] were referenced against runs performed with ligands alone to control for the heat of ligands solvation. The experiment was repeated keeping protein: protein and RNA: protein ratio same to make the comparison easy. Data are the mean of three independent experiments ± SD.

Cross-linking assay

Before glutaraldehyde cross-linking experiment, the protein was dialyzed in reaction buffer (20 mM HEPES pH 7.5 and 150 mM NaCl) to remove all the interfering molecules such as DTT and Tris. Two sets of samples (15 μl each), one containing 5 mM ATP and 50 μM *Vc*Rho and the other 5 mM ATP, 50 μM *Vc*Rho, and 100 μM *Vc*YaeO dimer, were prepared. Cross-linking was initiated by adding gluteraldehyde (Sigma-Aldrich) solution to a final concentration 0.25% (W/V) and quenched with 0.2 M ammonium acetate, pH 8.5. These cross-linked products were analyzed by SDS-PAGE to determine the oligomeric state of *Vc*Rho.

Dynamic light scattering

DLS experiments were performed by Malvern Zetasizer Nano S instrument (Malvern, Herremberg, Germany) equipped with a 633 nm He−Ne laser and operating at an angle of 173°. Data were collected for 50 μl sample volume having either 5 μM protein (*Vc*Rho_{FL}-hexamer) or 65 μM protein sample (5 μM *Vc*Rho_{FL}-hexamer + 60 μM *Vc*YaeO dimer) in the buffer (25 mM HEPES pH 7.5, 100 mM NaCl, 100 mM KCl) and in presence and absence of 5 mM ATP, using a micro quartz cuvette (Malvern-ZEN2112) at 20 °C. Protein samples were centrifuged at 12,000 rpm for 10 min and filtered serially through 0.22 μm Millipore syringe filter before each measurement. Each sample was incubated in the cuvette at 20 °C for 5 min in instrument sample chamber, set at 20 °C. Following incubation, three measurements were made consisting of 10 runs of 10 s each. Similarly, to determine the molar ratio of Rho monomer:YaeO dimer, which disrupts hexameric assembly of *Vc*Rho_{FL}, data were collected with increasing concentration of *Vc*YaeO dimer keeping the concentration of *Vc*Rho_{FL} monomer (constant 30 μM) in presence of 5 mM ATP/(5 mM ATP+ 20 μM $(dC)_{34}$). Data were analyzed using the software Zetasizer. The DLS results are expressed in terms of size distribution by volume. For the measurement of the hydrodynamic radius (R_h) of *Vc*Rho and *Vc*YaeO complex, the proteins were mixed in 1:6 ratios (*Vc*Rho-hexamer: *Vc*YaeO dimer). Data representing R_h are the mean of three independent measurements ±SD.

Intrinsic fluorescence quenching study with nucleotides and oligonucleotides

Steady-state fluorescence was measured using a VARIAN *Cary Eclipse* fluorescence spectrophotometer using 10 mm path length quartz cuvettes with 5 nm band pass slits for both excitation and emission channels. About 5 μM *Vc*YaeO was used in a final reaction volume of 0.8 ml for the nucleotides (GTP, CTP, ATP, and UTP) and oligonucleotides (dG_{12}, dC_{12}, rG_{12}, and rC_{12}) binding experiments. All the experiments were carried out in same buffer 25 mM HEPES pH 7.5, 50 mM NaCl, 50 mM KCl, and 2% glycerol. Nucleotides and oligonucleotides were purchased from Sigma-Aldrich and dissolved in autoclave water to a final concentration of 10 mM and 500 μM, respectively, and diluted as required in experiments. Tryptophan fluorescence was measured on excitation at 295 nm, and change in emission was measured at 340 nm. Binding constant was evaluated from the change in the fluorescence intensity of *Vc*YaeO (λ_{EX}—295 nm; λ_{EM}—340 nm) on progressive addition of small aliquots of nucleotides and oligonucleotides. Sample temperature was maintained at 20 °C for all experiments, and K_d values were determined as discussed before. All data are the mean of three independent experiments ±SD.

Modeling of *Vc*YaeO and *Vc*Rho interactions

To prepare the docked model of *Vc*YaeO:*Vc*Rho, a homology model of *Vc*Rho has been generated in SWISS-MODEL server [35]. Docking of *Vc*YaeO on the N-terminal part of *Vc*Rho was done by the HADDOCK server [36] using interaction restrain D36-K100, D36-K115, and E45-R88. The best model was chosen based on buried surface area and internal energy gained due to complex formation that was further fitted in Coot and geometry minimized. This minimized coordinate *Vc*YaeO:*Vc*Rho was used to generate the hexameric open- and closed-ring structures using the previously published coordinates of *Ec*Rho [37,38] as template.

Molecular dynamics simulation

Conventional MD simulation was carried out using the GPU version of AMBER 16 [39] and the ff14SB force field parameters for protein backbone and side chains. TIP3P water molecules were used to solvate the protein in a truncated octahedron box that extends up to 10 Å from the surface of the solute. The solvated system was neutralized by adding 16 Na^+ ions at random locations in the solvent. The periodic boundary condition was applied in all the directions. Bonds containing H-atoms were restrained with SHAKE algorithm [40], thus allowing us to choose a time step of 2 fs for the integrator. To control the temperature and pressure, a weak coupling to an external temperature and pressure bath was used [41]. The temperature control has been performed via Langevin dynamics [40], with a collision frequency of 2 ps^{-1}. Pressure control was accomplished by coupling the system to a Berendsen barostat at a reference pressure of 1 atm and with a relaxation time of 2 ps. The electrostatic interactions were calculated using the particle mesh Ewald summation [42] with a cutoff of 10 Å for the long-range interactions. The system was minimized for 500 steps using the steepest descent algorithm followed by another 1500 steps using the conjugate gradient algorithm. The minimization was done in two steps, first restraining the solute and allowing only the solvent to move and then turning off the restrains. The solvated system was then equilibrated for 5 ns in an isothermal-isovolumetric (NVT) ensemble, and the system was heated to 310 K. The final equilibration was achieved by a 5 ns isothermal-isobaric (NPT) simulation. The system was ensured to attain the correct temperature and density after the equilibration step. Finally, production run was carried out in the NPT ensemble for 650 ns. The contact area in Fig. 8c was calculated using *molsurf* of *cpptraj* in Amber.

Acknowledgments

This work was funded by the MSACR project, Department of Atomic Energy (DAE), Government of India.

Appendix A. Supplementary data

Supplementary data to this article can be found online at https://doi.org/10.1016/j.jmb.2019.09.019.

Received 11 July 2019;
Received in revised form 25 September 2019;
Accepted 26 September 2019
Available online 16 October 2019

Keywords:
X-ray crystallography;
Antitermination;
Fluorescence quenching;
ATPase;
Cell viability

References

[1] F.C. Neidhardt, R. Curtiss III, J.L. Ingraham, E.C.C. Lin, K.B. Low, B. Magasanik, W.S. Reznikoff, M. Riley, M. Schaechter, H.E. Umbarger, Escherichia coli and Salmonella: Cellular and Molecular Biology, 1996.

[2] V. Brendel, G.H. Hamm, E.N. Trifonov, Terminators of transcription with RNA polymerase from Escherichia coli: what they look like and how to find them, J. Biomol. Struct. Dyn. 3 (1986) 705–723, https://doi.org/10.1080/07391102.1986.10508457.

[3] T. Opperman, J.P. Richardson, Phylogenetic analysis of sequences from diverse bacteria with homology to the Escherichia coli rho gene, J. Bacteriol. 176 (1994) 5033–5043, https://doi.org/10.1128/jb.176.16.5033-5043.1994.

[4] T. Platt, Rho and RNA: models for recognition and response, Mol. Microbiol. 11 (1994) 983–990, https://doi.org/10.1111/j.1365-2958.1994.tb00376.x.

[5] J. Richardson, Structural organization of transcription termination factor Rho, J. Biol. Chem. 271 (1996) 1251–1254.

[6] B. Pani, S. Banerjee, J. Chalissery, M. Abishek, R.M. Loganathan, R.B. Suganthan, R. Sen, Mechanism of inhibition of Rho-dependent transcription termination by bacteriophage P4 protein Psu, J. Biol. Chem. (2006), https://doi.org/10.1074/jbc.M603982200.

[7] A. Ranjan, S. Sharma, R. Banerjee, U. Sen, R. Sen, Structural and mechanistic basis of anti-termination of Rho-dependent transcription termination by bacteriophage P4 capsid protein Psu, Nucleic Acids Res. 41 (2013) 6839–6856, https://doi.org/10.1093/nar/gkt336.

[8] R. Banerjee, S. Nath, A. Ranjan, S. Khamrui, B. Pani, R. Sen, U. Sen, The first structure of polarity suppression protein, Psu from enterobacteria phage P4, reveals a novel fold and a knotted dimer, J. Biol. Chem. 287 (2012) 44667–44675, https://doi.org/10.1074/jbc.M112.423202.

[9] S. Pichoff, L. Alibaud, A. Guédant, M.P. Castanié, J.P. Bouché, An Escherichia coli gene (yaeO) suppresses temperature-sensitive mutations in essential genes by modulating Rho-dependent transcription termination, Mol. Microbiol. 29 (1998) 859–869, https://doi.org/10.1046/j.1365-2958.1998.00981.x.

[10] P. Gutiérrez, G. Kozlov, L. Gabrielli, D. Elias, M.J. Osborne, I.E. Gallouzi, K. Gehring, Solution structure of YaeO, a rho-specific inhibitor of transcription termination, J. Biol. Chem. 282 (2007) 23348–23353, https://doi.org/10.1074/jbc.M702010200.

[11] K. Kavita, F. de Mets, S. Gottesman, New aspects of RNA-based regulation by Hfq and its partner sRNAs, Curr. Opin. Microbiol. (2018), https://doi.org/10.1016/j.mib.2017.10.014.

[12] M. Rabhi, O. Espéli, A. Schwartz, B. Cayrol, A.R. Rahmouni, V. Arluison, M. Boudvillain, The Sm-like RNA chaperone Hfq mediates transcription antitermination at Rho-dependent terminators, EMBO J. (2011), https://doi.org/10.1038/emboj.2011.192.

[13] A. Jutla, E. Whitcombe, N. Hasan, B. Haley, A. Akanda, A. Huq, M. Alam, R.B. Sack, R. Colwell, Environmental factors influencing epidemic cholera, Am. J. Trop. Med. Hyg. (2013), https://doi.org/10.4269/ajtmh.12-0721.

[14] L. Holm, P. Rosenström, Dali server: conservation mapping in 3D, Nucleic Acids Res. 38 (2010), https://doi.org/10.1093/nar/gkq366.

[15] J. Vogel, B.F. Luisi, Hfq and its constellation of RNA, Nat. Rev. Microbiol. (2011), https://doi.org/10.1038/nrmicro2615.

[16] V. Murina, N. Lekontseva, A. Nikulin, Hfq binds ribonucleotides in three different RNA-binding sites, Acta Crystallogr. D. Biol. Crystallogr. 69 (2013) 1504–1513, https://doi.org/10.1107/S090744491301010X.

[17] E. Krissinel, K. Henrick, Inference of macromolecular assemblies from crystalline state, J. Mol. Biol. 372 (2007) 774–797, https://doi.org/10.1016/j.jmb.2007.05.022.

[18] A.A. Baykov, O.A. Evtushenko, S.M. Avaeva, A malachite green procedure for orthophosphate determination and its use in alkaline phosphatase-based enzyme immunoassay, Anal. Biochem. 171 (1988) 266–270, https://doi.org/10.1016/0003-2697(88)90484-8.

[19] W. Wang, L. Wang, Y. Zou, J. Zhang, Q. Gong, J. Wu, Y. Shi, Cooperation of Escherichia coli Hfq hexamers in DsrA binding, Genes Dev. (2011), https://doi.org/10.1101/gad.16746011.

[20] T.M. Link, P. Valentin-Hansen, R.G. Brennan, Structure of Escherichia coli Hfq bound to polyriboadenylate RNA, Proc. Natl. Acad. Sci. U. S. A. (2009), https://doi.org/10.1073/pnas.0908744106.

[21] E.P. Gogol, S.E. Seifried, P.H. von Hippel, Structure and assembly of the Escherichia coli transcription termination factor rho and its interactions with RNA I. Cryoelectron microscopic studies, J. Mol. Biol. (1991), https://doi.org/10.1016/0022-2836(91)90923-T.

[22] F. Corpet, Multiple sequence alignment with hierarchical clustering, Nucleic Acids Res. 16 (1988) 10881–10890, https://doi.org/10.1093/nar/16.22.10881.

[23] J. Jancarik, S.H. Kim, Sparse matrix sampling. A screening method for crystallization of proteins, J. Appl. Crystallogr. 24 (1991) 409–411, https://doi.org/10.1107/S0021889891004430.

[24] A. Kumar, B. Ghosh, H.K. Poswal, K.K. Pandey, Jagannath, M.V. Hosur, A. Dwivedi, R.D. Makde, S.M. Sharma, Protein crystallography beamline (PX-BL21) at Indus-2 synchrotron, J. Synchrotron Radiat. (2016), https://doi.org/10.1107/S160057751600076X.

[25] W. Kabsch, XDS, Acta Crystallogr. D. Biol. Crystallogr. 66 (2010) 125–132, https://doi.org/10.1107/S0907444909047337.

[26] B.W. Matthews, Solvent content of protein crystals, J. Mol. Biol. 33 (1968) 491–497, https://doi.org/10.1016/0022-2836(68)90205-2.

[27] M.D. Winn, C.C. Ballard, K.D. Cowtan, E.J. Dodson, P. Emsley, P.R. Evans, R.M. Keegan, E.B. Krissinel, A.G.W. Leslie, A. McCoy, S.J. McNicholas, G.N. Murshudov, N.S. Pannu, E.A. Potterton, H.R. Powell, R.J. Read, A. Vagin, K.S. Wilson, Overview of the CCP4 suite and current developments, Acta Crystallogr. D. Biol. Crystallogr. (2011), https://doi.org/10.1107/S0907444910045749.

[28] P.D. Adams, P.V. Afonine, G. Bunkóczi, V.B. Chen, I.W. Davis, N. Echols, J.J. Headd, L.W. Hung, G.J. Kapral, R.W. Grosse-Kunstleve, A.J. McCoy, N.W. Moriarty, R. Oeffner, R.J. Read, D.C. Richardson, J.S. Richardson,

T.C. Terwilliger, P.H. Zwart, PHENIX: a comprehensive Python-based system for macromolecular structure solution, Acta Crystallogr. D. Biol. Crystallogr. 66 (2010) 213–221, https://doi.org/10.1107/S0907444909052925.
[29] P. Emsley, K. Cowtan, Coot: model-building tools for molecular graphics, Acta Crystallogr. D. Biol. Crystallogr. 60 (2004) 2126–2132, https://doi.org/10.1107/S0907444904019158.
[30] E.F. Pettersen, T.D. Goddard, C.C. Huang, G.S. Couch, D.M. Greenblatt, E.C. Meng, T.E. Ferrin, UCSF Chimera – a visualization system for exploratory research and analysis, J. Comput. Chem. (2004), https://doi.org/10.1002/jcc.20084.
[31] O.H. Lowry, N. j Rosebrough, R.J. Randall, A. Lewis, Protein measurement with folin phenol reagent, Biol. Chem. (1951), https://doi.org/10.1016/0304-3894(92)87011-4.
[32] A.G. To, F. Probes, L. Technologies, The molecular Probes® handbook, Mol. Probes® Handb. (2010) 99–121. http://www.lifetechnologies.com/tr/en/home/references/molecular-probes-the-handbook.html.
[33] S. Chakrabarti, P. Roy, D. Dasgupta, Interaction of the antitumor antibiotic chromomycin A3 with glutathione, a sulfhydryl agent, and the effect upon its DNA binding properties, Biochem. Pharmacol. 56 (1998) 1471–1479, https://doi.org/10.1016/S0006-2952(98)00249-4.
[34] G. Ghosh, J. Reddy, S. Sambhare, R. Sen, A bacteriophage capsid protein is an inhibitor of a conserved transcription terminator of various bacterial pathogens, J. Bacteriol. 200 (2018) 1–16, https://doi.org/10.1128/JB.00380-17.
[35] T. Schwede, J. Kopp, N. Guex, M.C. Peitsch, SWISS-MODEL: an automated protein homology-modeling server, Nucleic Acids Res. 31 (13) (2003) 3381–3385, https://doi.org/10.1093/nar/gkg520.
[36] G.C.P. Van Zundert, J.P.G.L.M. Rodrigues, M. Trellet, C. Schmitz, P.L. Kastritis, E. Karaca, A.S.J. Melquiond, M. Van Dijk, S.J. De Vries, A.M.J.J. Bonvin, The HADDOCK2.2 web server: user-friendly integrative modeling of biomolecular complexes, J. Mol. Biol. (2016), https://doi.org/10.1016/j.jmb.2015.09.014.
[37] E. Skordalakes, J.M. Berger, Structure of the Rho transcription terminator: mechanism of mRNA recognition and helicase loading, Cell (2003), https://doi.org/10.1016/S0092-8674(03)00512-9.
[38] N.D. Thomsen, J.M. Berger, Running in reverse: the structural basis for translocation polarity in hexameric helicases, Cell (2009), https://doi.org/10.1016/j.cell.2009.08.043.
[39] D.A. Case, R. Betz, W. Botello-Smith, D.S. Cerutti, T.E. Cheatham, T.A. Darden, R.E. Duke, T.J. TGiese, H. Gohlke, A.W. Goetz, N. Homeyer, S. Izadi, P. Janowski, J. Kaus, A. Kovalenko, T.S. Lee, AMBER 2016, Univ. California, San Fr, 2016, https://doi.org/10.1021/ct200909j.
[40] J.P. Ryckaert, G. Ciccotti, H.J.C. Berendsen, Numerical integration of the cartesian equations of motion of a system with constraints: molecular dynamics of n-alkanes, J. Comput. Phys. (1977), https://doi.org/10.1016/0021-9991(77)90098-5.
[41] H.J.C. Berendsen, J.P.M. Postma, W.F. Van Gunsteren, A. Dinola, J.R. Haak, Molecular dynamics with coupling to an external bath, J. Chem. Phys. (1984), https://doi.org/10.1063/1.448118.
[42] U. Essmann, L. Perera, M.L. Berkowitz, T. Darden, H. Lee, L.G. Pedersen, A smooth particle mesh Ewald method, J. Chem. Phys. (1995), https://doi.org/10.1063/1.470117.